Materials Science and Engineering B 295 (2023) 116585

Contents lists available at ScienceDirect

Materials Science & Engineering B

journal homepage: www.elsevier.com/locate/mseb

Two-layer hybrid sol-gel system's thermal parameters investigated with the optical nondestructive photoacoustic method in the frequency domain

Łukasz Chrobak [a], Mirosław Maliński [a], Dorota Korte [b]

[a] Koszalin University of Technology, Faculty of Electronics and Computer Science, Śniadeckich 2, 75-453 Koszalin, Poland
[b] University of Nova Gorica, Laboratory for Environmental and Life Sciences, Vipavska cesta 13, Nova Gorica 5000, Slovenia

ARTICLE INFO

Keywords:
Optical spetroscopy
Nondestructive testing
Photoacoustic method
Thermal parameters
Hybrid sol–gel layers
Thin film characterization

ABSTRACT

This work presents results of studies of thermal parameters such as thermal diffusivity, thermal conductivity, thermal effusivity and volumetric heat capacity of thin hybrid sol-gel corrosion protective layers deposited on the aluminum substrate. In the studies two groups of samples were investigated. The first group was: TMZ.1, TMZ.2 and TMZ.3 (TMZ- Si/Zr-based hybrid sol-gel coatings), with different amount of zirconium, and the second group was: TMZ.1/Ce, TMZ.2/Ce and TMZ.3/Ce (TMZ/Ce - Ce-doped Si/Zr-based hybrid sol-gel coatings) with the same amount of zirconium and an addition of cerium. This work presents the influence of the content of zirconium and cerium on their thermal parameters. The possibility of using the nondestructive photoacoustic method (PA), with the microphone detection, to characterize this type of layers was analyzed theoretically and experimentally too.

1. Introduction

Aluminum and its alloys are of high interest and have already gained a broad spectrum of applications due to their physical characteristics. Aluminum alloys are highly susceptible to oxidation and pitting corrosion in aggressive environments. Various coating materials are used to protect such kind of materials under different service conditions. In general the issue of the sol gel coatings as a corrosion protective coatings is described in papers [1–4]. It has been reported that amorphous, homogeneous coatings containing Si and Zr and polymerized organic matrix provide high corrosion resistance for aluminum and aluminum alloys, even under aggressive conditions [5,6]. The degree of protection is dependent on the Zr content in the coating. Cerium salts, e.g. chloride, acetate and nitrate, are recognized as efficient corrosion inhibitors for Al-based alloys when added directly in the corrosive medium [7,8]. For this reason, the Ce-doped Si/Zr-based hybrid sol–gel coatings are interesting [9]. It has been reported that in the Si/Zr-based hybrid sol–gel different amounts of zirconium in the siloxane network and the addition of cerium into Si/Zr sol coatings are reflected in the values of material thermal properties [10]. The differences in their thermal parameters are attributed to the difference in structure and nano-organization of the formed Si/Zr complexes. The first aim of this paper was to check in detail changes in the thermal parameters caused by the composition of the Ce-doped Si/Zr-based hybrid sol–gel coatings.

The second aim was to examine the possibilities of using the nondestructive PA method to determine this parameters of investigated coatings. Since the eighties, a large progress has been made in the investigations of the use of different non-destructive photothermal methods. All these measurement methods have found wide applications in the investigations of different parameters of materials. For determination of thermal parameters different methods are applied. Among them the most frequently used methods are photothermal methods: photoacoustic (PA) [11–19], photothermal radiometric (PTR) [20–25], beam deflection spectroscopy (BDS) [26–30], piezoelectric method (PZE) [31–36] and photopyroelectric (PPE) [37–40]. In most cases thermal parameters are determined for single layer structures. For determination of thermal parameters of two layer structures the problem becomes much more complicated. It needs theoretical models of the photothermal signals [41,42]. This paper is the presentation of the theoretical and experimental approach, in the frame of the photoacoustic (PA) method in the frequency domain, for determination of the thermal parameters such as: thermal diffusivity, thermal conductivity, thermal effusivity and heat capacity of thin coating layers deposited on the thick aluminum substrate.

E-mail addresses: lukasz.chrobak@tu.koszalin.pl (Ł. Chrobak), miroslaw.malinski@tu.koszalin.pl (M. Maliński), dorota.korte@ung.si (D. Korte).

https://doi.org/10.1016/j.mseb.2023.116585
Received 20 February 2023; Received in revised form 27 April 2023; Accepted 16 May 2023

2. Materials

- 1 mm-thick flat aluminum sheet (Aluminum (>99.0%, GoodFellow, England),
- -tetraethyl orthosilicate (TEOS: $Si(OC_2H_5)_4$, 99.9%, Aldrich, Munich, Germany),
- 3-methacryloxypropyltrimethoxysilane (MAPTMS: $H_2C = C(CH_3)CO_2(CH_2)3Si(OCH_3)_3$, ≥98%, Sigma, St. Louis, MO, USA),
- zirconium tetrapropoxide, (ZTP: $Zr(OCH_2CH_2CH_3)_4$, 70 wt%, in 1-propanol, Aldrich, St. Louis, MO, USA),
- methacrylic acid (MAA: $H_2C = C(CH_3)COOH$, 99.0%, Aldrich, Zwijndrecht, The Netherlands),
- hydrochloric acid (HCl, >37%, AppliChem, Darmstadt, Germany).
- sols were doped with 0.5 wt% of cerium(III) nitrate hexahydrate ($Ce(NO_3)_3{\cdot}6H_2O$, 99.9%, Sigma, Lyon, France).

The coatings were prepared by sol–gel method with TEOS, MAPTMS, ZTP and MAA precursors. The molar ratio of the applied precursors TEOS/MAPTMS/ZTP/MAA was 0.18:1:X:0.12. X was 0.06, 0.12 and 0.48. The amounts of H_2O (2.075 mol) and catalyst HCl (0.001 mol) were kept constant during sample preparations. Such prepared sols-gel coatings have been denoted as TMZ.1, TMZ.2 and TMZ.3. TMZ.1 had the smallest and TMZ.3 the largest amount of ZTP. The TMZ sols were next modified. The 0.5 wt% of $Ce(NO_3)_3$ was added into sol and the solution was stirred for 10 min. The clear sol was then aged for 1 h. Sols samples with an addition of Cerium have been denoted as TMZ.1/Ce, TMZ.2/Ce and TMZ.3/Ce. These sols were next deposited on the aluminum, 1 mm thick, discs by the use of a spin-coater rotated at 4000 rpm for 30 s after which they were left for resting for 10 min at ambient conditions and finally thermally cured at 100 °C for one hour in the presence of daylight. The coatings, with a thickness of about 10 μm which were prepared this way, were homogeneous, transparent, colorless and free of cracks. Details about the procedure of sample preparation can be found in [43].

3. Thermal model

The PA method, for single layers, is based on the theory of the photoacoustic effect with solids [11] and the thermal wave interferometric method [12]. In this method the sample is illuminated with the periodically modulated intensity of the beam of light. As a result the periodical temperature of the illuminated surface of the sample arises. This temperature causes periodical changes of the overpressure of gas in the photoacoustic chamber which are detected by a microphone. This experimental front configuration is presented schematically in Fig. 1. The calculations of the PA signal of the investigated samples have been performed in the two layer model [44]. The schematic drawing of the investigated samples is also presented in Fig. 1.

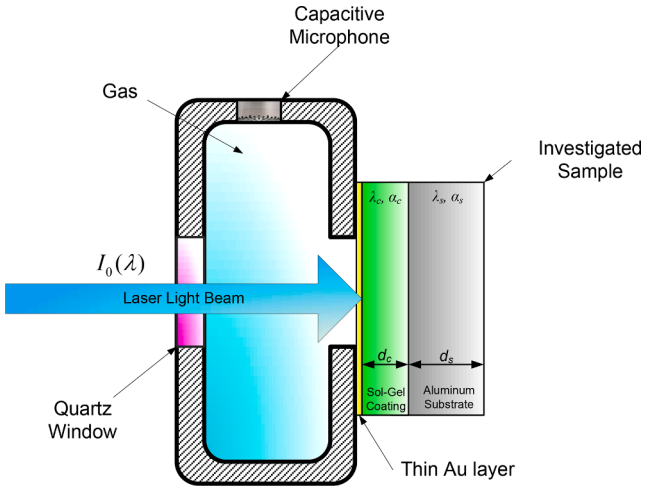

Fig. 1. Schematic drawing of the investigated sample in the PA cell under the laser beam excitation.

The 10 μm thick sol–gel coating was deposited on the aluminum substrate. This structure was covered with the thin layer of gold of the thickness of a few nanometers. The layer of gold was the light absorber which is optically thick and thermally thin. In this way the sol–gel coating could be treated as two layer, optically opaque structure.

The temperature of the illuminated surface of the sample can be expressed by formula (1) and is described in [44].

$$T = \frac{I}{\lambda_c \cdot \sigma_c} \cdot \frac{\cosh(d_c \cdot \sigma_c + d_s \cdot \sigma_s) + R_{12} \cdot \cosh(d_c \cdot \sigma_c - d_s \cdot \sigma_s)}{\sinh(d_c \cdot \sigma_c + d_s \cdot \sigma_s) + R_{12} \cdot \sinh(d_c \cdot \sigma_c - d_s \cdot \sigma_s)} \tag{1}$$

where:

I - laser light intensity [W/cm^2];

R_{12} - thermal reflection coefficient between the coating and the substrate [1];

d_i - thickness [cm];

λ_i - thermal conductivity [W/cmK];

α_i - thermal diffusivity [cm^2/s];

Subscript i can be c, s and g what refers to the coating, substrate and the gas respectively.

The thermal reflection coefficient between the coating and the substrate is described by Eq.2:

$$R_{12} = \frac{\frac{\lambda_c}{\sqrt{\alpha_c}} - \frac{\lambda_s}{\sqrt{\alpha_s}}}{\frac{\lambda_c}{\sqrt{\alpha_c}} + \frac{\lambda_s}{\sqrt{\alpha_s}}} \tag{2}$$

The complex thermal wave number σ_i, (subscript i can be s, c and g what refers to the coating, the substrate and the gas respectively) is described by Eq.3:

$$\sigma_i = (1+i)\sqrt{\frac{\Pi f}{\alpha_i}} \tag{3}$$

where:

f – frequency modulation of the laser beam intensity.

The pressure in the photoacoustic cell, marked as PA, related to the temperature of the sample surface described by equation (1), is given as:

$$PA = T/\sigma_g \tag{4}$$

The amplitude and phase of the pressure, related to the temperature of the sample surface described by equation (1), are given by formulas (5) and (6).

$$Amp(PA) = |PA| \tag{5}$$

$$Ph(PA) = \frac{180}{\pi} \cdot \arg(PA) \tag{6}$$

The theoretical frequency characteristics of the PA signal of the two layer optically opaque structure are presented in Fig. 2. They show how thermal diffusivity and conductivity affect the frequency PA amplitude and phase characteristics. The values of parameters taken for the simulations were as follows: $d_c = 10{\cdot}10^{-4}$ cm, $d_s = 0.05$ cm, $\alpha_c = 5.0{\cdot}10^{-3}$ cm^2/s, $\lambda_c = 2.0{\cdot}10^{-3}$ W/cm·K, $\alpha_s = 0.973$ cm^2/s, $\lambda_s = 2.37$ W/cm·K.

It can be seen that with the increase of the thermal conductivity and thermal diffusivity of the coating, both amplitude and phase characteristics shift towards higher frequencies. From the fitting of the theoretical frequency PA characteristics to the experimental PA characteristics both the thermal diffusivity and thermal conductivity can be determined.

The characteristic frequency for the coating (f_{cc}), for which the thermal wave diffusion length is equal to the thickness of the coating, can be expressed as follows:

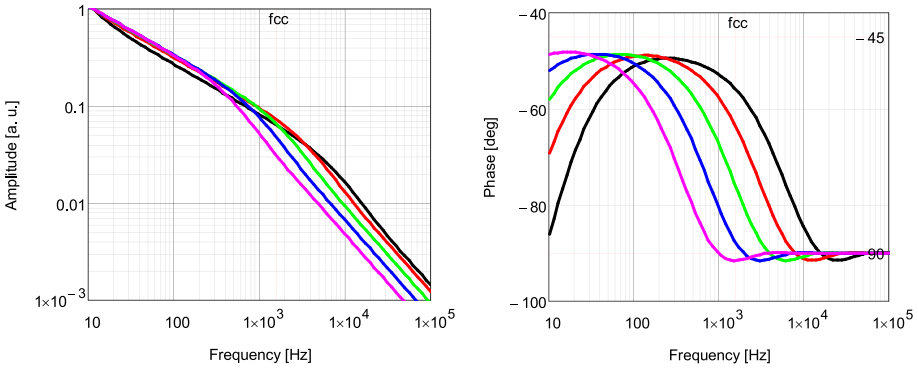

Fig. 2. Theoretical photoacoustic PA(f) amplitude and phase characteristics calculated for different values of thermal parameters. Solid green line (α_c, λ_c), solid red line ($2{\cdot}\alpha_c$, $2{\cdot}\lambda_c$), solid black line ($4{\cdot}\alpha_c$, $4{\cdot}\lambda_c$), solid blue line ($\alpha_c/2$, $\lambda_c/2$) and solid pink line ($\alpha_c/4$, $\lambda_c/4$).

$$f_{cc} = \frac{\alpha_c}{\pi \cdot d_c} \tag{6}$$

With an increase of the thermal diffusivity of the coating, the corresponding value of the characteristic frequency for the coating (f_{cc}) moves towards higher frequencies. This situation is presented in Fig. 2. The theoretical frequency phase *PA* characteristics are more sensitive for changes of the thermal parameters of the coating layer than the amplitude *PA* characteristics. The 4 times increase of the thermal diffusivity of the coating, and also of its thermal conductivity, changes the value of the characteristic frequency 4 times i.e. from for example $2{\cdot}10^3$ Hz to $8{\cdot}10^3$ Hz. Low range of frequencies is dominated by the thermal parameters of the aluminum substrate.

4. Samples description

The examined coatings consist of inorganic metal alkoxides and organic alkoxides that include a network-forming element as Zr, Ce. A formed gel network contain condensed inorganic M−O−M (M is Si, Zr) and polymerized organic M−R−R_n' moieties (R is an alkyl group and R_n' is carbon chain containing functional group, e.g. epoxy, acrylate, amino, etc.). To induce the condensation reactions it is necessary to add Zr to hydrolysed siloxane sol. In such a way larger silicon domains are formed what results in a higher degree of polycondensation. Such coatings are very promising as corrosion protection materials since they are easy to be prepared with low costs, present a dense structure and good homogenity that was achieved through condensation reactions between Si- and Zr-based precursors [45–46]. The performed SEM analysis indicates that the coatings are very compact, without pores and the state of homogeneity improves with the increase in the amount of zirconium in the coating (Fig. 3). The addition of cerium salt to the solution causes the decrease in its pH accelerating the same time the gelation process of the sols what could result in increase in the cracking susceptibility of the hybrid coating and lead to decrease in the coating corrosion performance. Thus, the control of amount of Ce added to the coating must be performed to obtain dense, homogeneous layers without cracks containing Ce that acts as corrosion inhibitor and improves corrosion resistance of the coating by blocking the corrosion activity of the damaged surface through the formation of products with enhanced barrier properties.

[47]. The thickness of such synthesized coatings do not differ significantly within the range of its determination uncertainty.

The FTIR spectra of the hydrolysed sol, recorded at intervals of 1 min in the range of 600–2800 cm^{-1}, confirm the occurrence of hydrolysis and condensation reactions of Si/Zr hybrid sols and formation of networks between MAPTMS and TEOS. Furthermore, the addition of zirconia and/or cerium influence on the degree of condensation in the

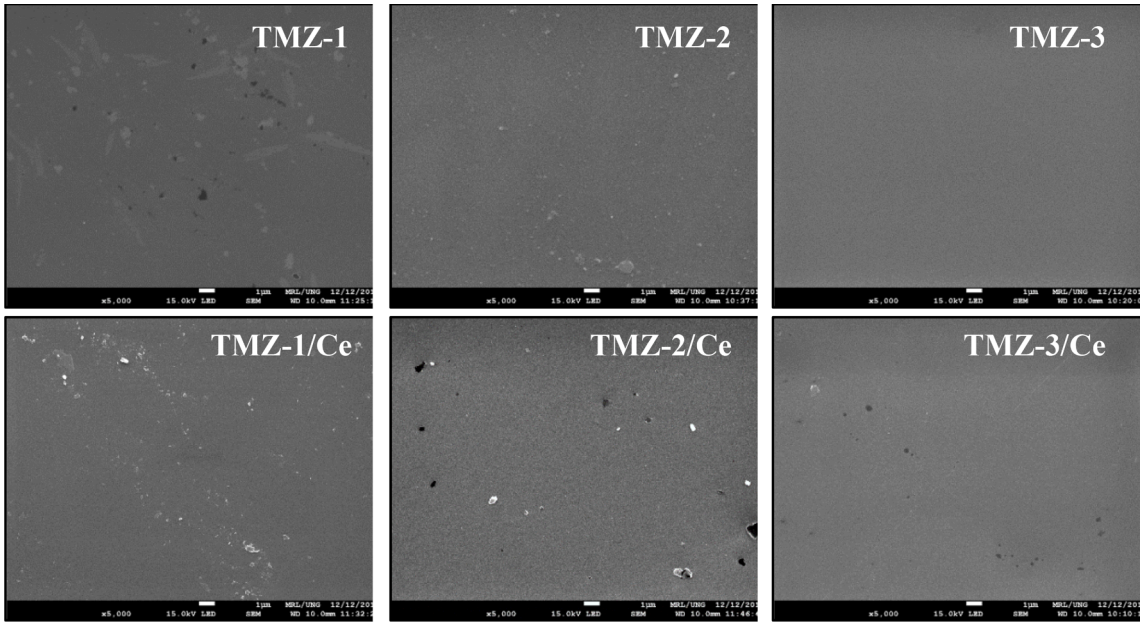

Fig. 3. The SEM images (5,000 ×) of the TMZ samples.

siloxane network that determines their structural and related properties [48–50].

5. Experimental results

The PA characteristics were measured on the PA set-up presented in Fig. 4.

The samples were placed in a photoacoustic cell and measured in the front configuration. The thermal waves were excited with the beam of the laser light using a laser diode Roithner LaserTechnik LD-450-1600MG with a beam size smaller than 1 mm, the output power 300 mW and a photon energy 2.76 eV corresponding to the operating wavelength $\lambda = 450$ nm. A Stanford Rese arch Systems lock-in amplifier SR830 was used for phase sensitive measurements and for the modulation of the intensity of the laser beam. The self designed photoacoustic cell (Helmholtz resonator) with a G.R.A.S. microphone (type 26AK) was used as a detector of the photoacoustic signal. Modeling and a design aspects of the photoacoustic cells were described in papers [51–55]. Measurements were fully automated and computer controlled. The set-up was controlled by an original application written in the high-level C++ language, in which the necessary control and acquisition algorithms were implemented. The frequency PA characteristics were measured in the wide frequency range from 10 Hz to 100 kHz. The intensity of the exciting laser light was modulated by the Thorlabs LDC205C Benchtop LD Current Driver.

There are advantages and disadvantages of this experimental method. The advantages: low cost of the experimental set-up, relatively simple model of the measured signal. The disadvantages: limited frequency of modulation caused by the microphone response band, resonances of the photoacoustic cell.

Experimental PA amplitude and phase characteristics of investigated samples are presented in Figs. 5-10. Circles are experimental data, solid lines are theoretical characteristics.

The experimental and theoretical amplitude and phase PA characteristics presented in Figs. 5-10 for TMZ and TMZ/Ce samples show that they are very similar. It means that the values of thermal parameters of the samples do not differ considerably. The measurement results are reproducible. Only the fitting procedures applied for the interpretation of the amplitude and phase characteristics indicated small differences in the values of thermal parameters of the samples.

The obtained values of the thermal parameters of investigated samples are presented in Tables 1 and 2. These values have been estimated using the best fits of Eqs.4 and 5 to the normalized experimental data with the use of the least-squares method (multi-parameter fittings). These values which have been obtained for investigated samples hold within the relative expanded uncertainties with 95.45 % ($\pm 2\sigma$) confidence level [56–57]. The values of thermal parameters of the aluminum substrate used for fittings were $\alpha_s = 0.973$ cm^2/s, $\lambda_s = 2.37$ W/cm·K.

Obtained values of the thermal diffusivities and thermal conductivities of TMZ samples are in good agreement with values obtained by other experimental methods i.e. PTR and BDS and presented in paper [58]. The obtained results clearly show that the applied PA method is equally attractive from the point of view of characterizing thin layers of the sol–gel type, such as, for example, the BDS or PTR methods.

Values of the thermal effusivities e_c (7) and volumetric heat capacities c_{vol} (8) computed from the values of thermal diffusivities and thermal conductivities of investigated coatings as:

$$e_c = \frac{\lambda_c}{\sqrt{\alpha_c}} \tag{7}$$

$$c_{vol} = \frac{\lambda_c}{\alpha_c} \tag{8}$$

are presented in Table 2.

It is seen from the obtained results that the addition of Zr into the siloxane structure results in the decrease in thermal properties of the materials. Zr is built into the coating structure as the network-forming element enabling the occurrence of condensation reactions. On the other hand, its incorporation introduces additional interfaces what increases the heat dissipation, thus, leading to decrease in the value of its thermal properties. Doping the coating with Ce changes the conditions of the sols gelation process and thus, makes the material more tend to cracks formation what leads to decrease in thermal properties comparing to the coating without an addition of Ce.

It can be concluded that the different amounts of zirconium in the siloxane network and the addition of cerium ions into Si/Zr sol are reflected in the different values of thermal properties that are related to the changes in the structure and nano-organization of the Si/Zr material. It means that the properties of the examined coatings are related to the combined effect of a more condensed Si − O − Zr network structure and the inhibiting effect of cerium ions. The synergetic effect of Zr and Ce ions introduced into the hybrid coating structure makes Ce to act both as inhibiting agent and as network-forming element producing the protection layer for the underlying Al substrate.

6. Conclusions

In this paper the values of all thermal parameters of corrosion protective hybrid sol–gel coatings, deposited on the aluminum substrate, such as: thermal conductivity, thermal diffusivity, thermal effusivity and volumetric heat capacity have been presented. These results have been obtained by the photoacoustic (PA) method in the frequency domain. The experimental results show that different content of Zr in the siloxane network and the addition of Ce into Si/Zr sols are reflected in the change of the values of their thermal parameters. It was proved that it was possible to determine simultaneously both thermal diffusivity and thermal conductivity of the samples from the fitting of theoretical to experimental frequency amplitude and phase PA characteristics. For this purpose the multiparameter fitting procedure was applied.

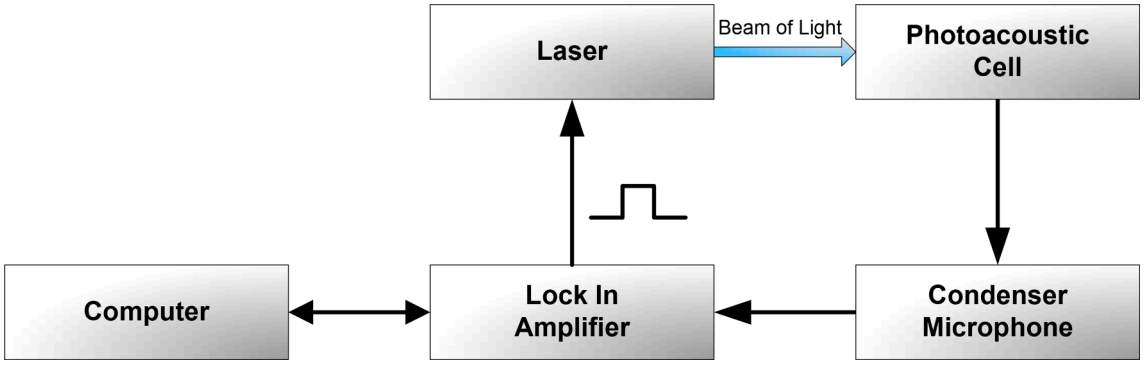

Fig. 4. Block diagram of the experimental set-up used for the measurements of the PA frequency characteristics.

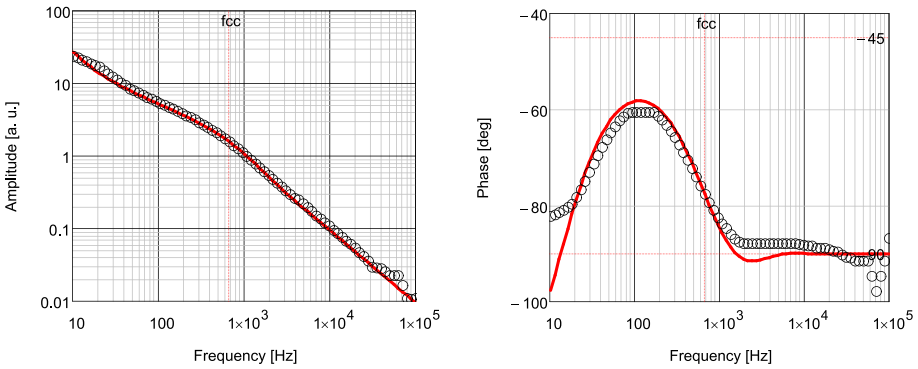

Fig. 5. Photoacoustic frequency, amplitude and phase, characteristics of TMZ.1 samples.

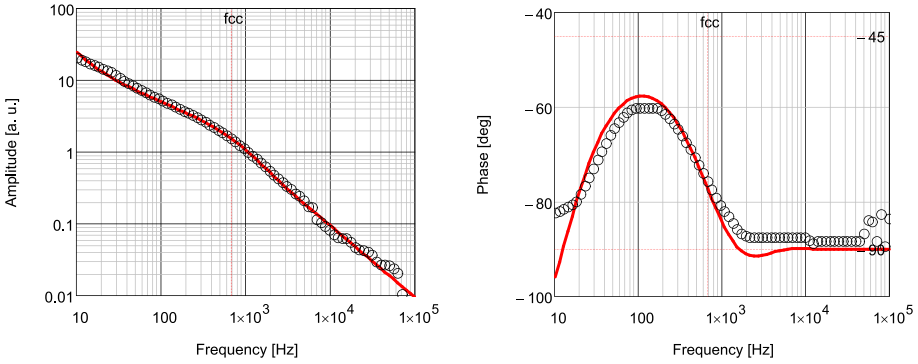

Fig. 6. Photoacoustic frequency, amplitude and phase, characteristics of TMZ.1/Ce samples.

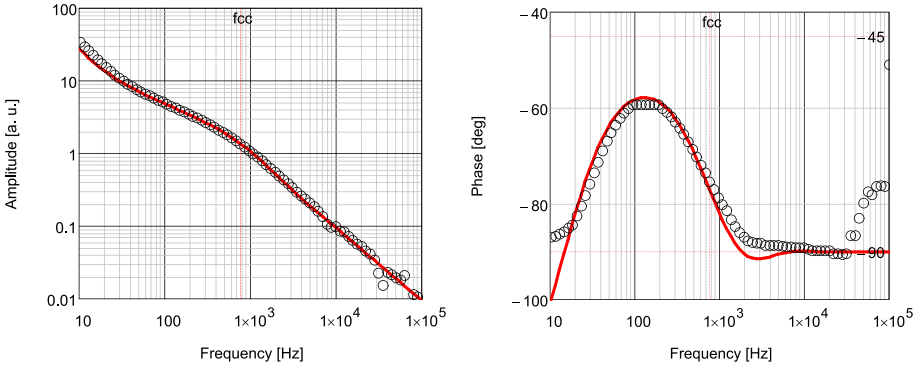

Fig. 7. Photoacoustic frequency, amplitude and phase, characteristics of TMZ.2 samples.

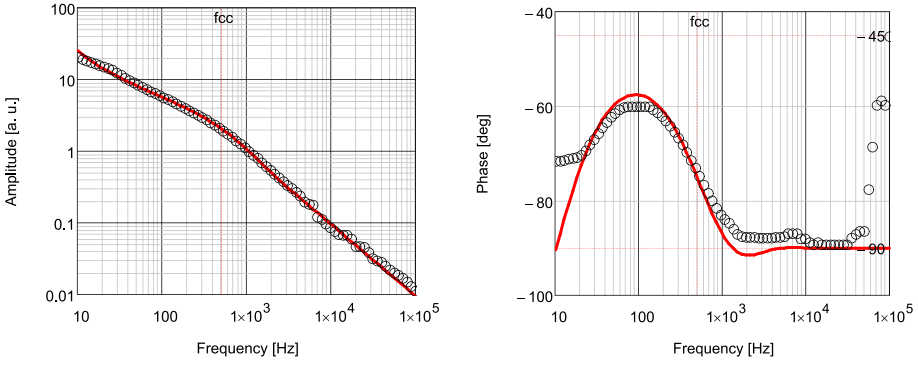

Fig. 8. Photoacoustic frequency, amplitude and phase, characteristics of TMZ.2/Ce samples.

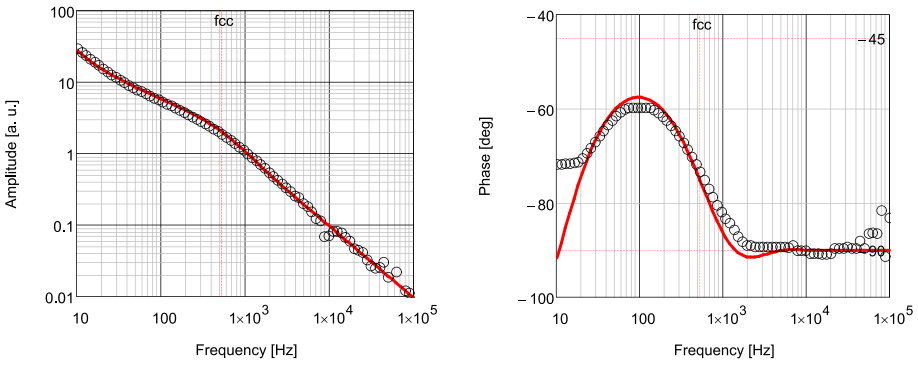

Fig. 9. Photoacoustic frequency, amplitude and phase, characteristics of TMZ.3 samples.

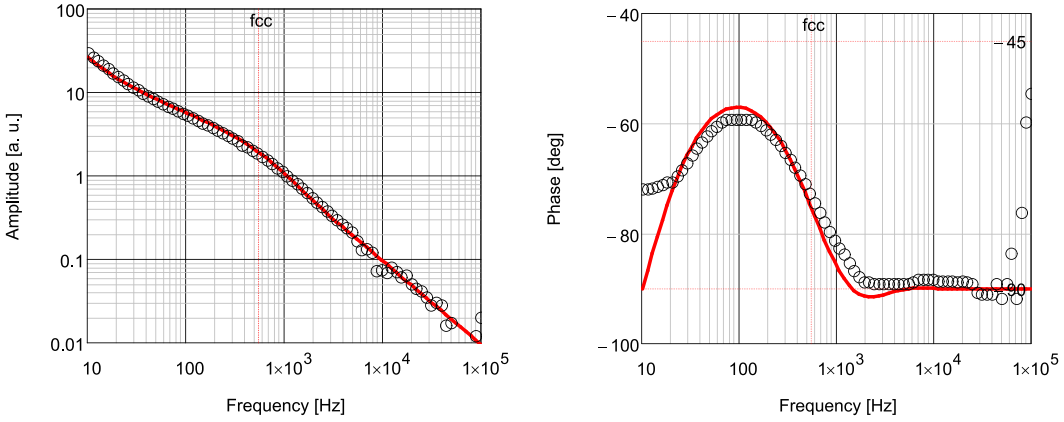

Fig. 10. Photoacoustic frequency, amplitude and phase, characteristics of TMZ.3/Ce samples.

Table 1
Values of thermal parameters of investigated coatings determined by the use of the PA method.

Material/Coating	Thermal Diffusivity $\alpha_c \times 10^{-3}\ \left[\frac{cm^2}{s}\right]$	Thermal Conductivity $\lambda_c \times 10^{-3}\ \left[\frac{W}{cmK}\right]$
TMZ.1	2.40 ± 0.13	2.59 ± 0.13
TMZ.1/Ce	2.13 ± 0.10	2.09 ± 0.11
TMZ.2	2.31 ± 0.21	2.37 ± 0.20
TMZ.2/Ce	2.01 ± 0.11	1.90 ± 0.12
TMZ.3	2.15 ± 0.09	2.20 ± 0.09
TMZ.3/Ce	1.83 ± 0.08	1.71 ± 0.10

Table 2
Values of the thermal effusivities and volumetric heat capacities of investigated coatings.

Material/Coating	Thermal Effusivity $e_c \times 10^{-3}\ \left[\frac{W\sqrt{s}}{cm^2K}\right]$	Volumetric Heat Capacity $c_{vol}\ \left[\frac{J}{cm^3K}\right]$
TMZ.1	52.84 ± 4.13	0.93 ± 0.10
TMZ.1/Ce	45.22 ± 3.50	1.02 ± 0.10
TMZ.2	49.33 ± 6.40	0.98 ± 0.17
TMZ.2/Ce	42.28 ± 3.86	1.06 ± 0.13
TMZ.3	47.53 ± 2.98	0.98 ± 0.08
TMZ.3/Ce	39.89 ± 3.26	1.07 ± 0.11

- The thermal diffusivity values obtained for the TMZ.1 - TMZ.3 samples are in the range of (2.40–2.15) · 10^{-3} cm^2/s.
- The thermal conductivity values of the same samples are in the range of (2.59–2.20) · 10^{-3} W/cm·K.
- The thermal effusivity values, computed from the values of thermal diffusivity and thermal conductivity values, are in the range (52.84 – 47.53)·10^{-3} $W\sqrt{s}/cm^2K$.
- The volumetric heat capacity value of the coatings, also computed from the values of thermal diffusivity and thermal conductivity, equals approximately to 1 J/cm^3K and is practically independent on the composition of the coatings.

From the obtained experimental results one can draw a conclusion that the thermal diffusivity, thermal conductivity and thermal effusivity of the samples (from TMZ.1 – to TMZ.3) decrease with an increase of the content of Zr in the sol–gel coating. These changes are however small. Thermal diffusivity decreased by 10 % while the thermal conductivity decreased by 15 %.

- Thermal diffusivity values obtained for the TMZ.1/Ce - TMZ.3/Ce samples are in the range of (2.13 – 1.83) · 10^{-3} cm^2/s.
- The thermal conductivity values of the samples are in the range of (2.09 – 1.71) · 10^{-3} W/cm·K.
- The thermal effusivities of these samples are in the range (45.22–39.89)·10^{-3} $W\sqrt{s}/cm^2K$.
- Volumetric heat capacity equals approximately to 1 J/cm^3K and is practically independent on the composition of the coatings.

The above parameters also decrease with the increase of Cr content in the sol–gel coatings. These changes of thermal parameters are however small. Thermal diffusivity decreased by 14 % while the thermal conductivity decreased by 18 %. The main goal of zirconium doping of the coatings is obtaining the high level of the corrosion protection. Cerium salts are efficient corrosion inhibitors. Addition of zirconium and cerium determines the structural properties of the coatings. The

obtained results show that increasing the content of zirconium and cerium can lead to the decrease of the thermal parameters of the coatings what can be associated with the structural defects in the coatings. This decrease is however not considerable which may indirectly indicate good structural properties of the sol–gel coatings.

The presented results also prove that the nondestructive PA method is definitely very attractive from the point of view of characterization of these sol–gel coatings. It is also one of the cheapest method of the thermal characterization of solid materials.

Declaration of Competing Interest

The authors declare that they have no known competing financial interests or personal relationships that could have appeared to influence the work reported in this paper.

Data availability

Data will be made available on request.

References

[1] P. Rodič, J. Iskra, I. Milošev, Study of a sol-gel process in the preparation of hybrid coatings for corrosion protection using FTIR and 1H NMR methods, J. Non Cryst. Solids 396–397 (2014) 25–35.

[2] D. Associates, J. R. Davis, Alloying: understanding the basics, Choice Reviews Online (2013), https://doi.org/10.5860/choice.39-5209.

[3] M.L. Zheludkevich, I. Miranda Salvado, M.G.S. Ferreira, Sol–gel coatings for corrosion protection of metals, J. Mater. Chem. 15 (2015) 5099–5111.

[4] D. Wang, G.P. Bierwagen, Sol–gel coatings on metals for corrosion protection, Prog. Org. Coat. 64 (4) (2009) 327–338.

[5] P. Rodič, I. Milošev, Corrosion properties of UV cured hybrid sol-gel coatings on AA7075-T6 determined under simulated aircraft conditions, J. Electrochem. Soc. 161 (9) (2014) C412–C420.

[6] P. Rodič, I. Milošev, Electrochemical and salt spray testing of hybrid coatings based on Si and Zr deposited on aluminum and its alloys, J. Electrochem. Soc. 162 (10) (2015) C592–C600.

[7] P. Rodič, A. Mertelj, M. Borovšak, A. Benčan, D. Mihailović, B. Malič, I. Milošev, Composition, structure and morphology of hybrid acrylate-based sol–gel coatings containing Si and Zr composed for protective applications, Surf. Coat. Technol. 286 (2016) 388–396.

[8] P. Rodič, I. Milošev, Corrosion Inhibition of Pure Aluminium and Alloys AA2024-T3 and AA7075-T6 by Cerium(III) and Cerium(IV) Salts, J. Electrochem. Soc. 163 (3) (2016) C85–C93.

[9] R.B. Figueira, C.J.R. Silva, E.V. Pereira, Organic–inorganic hybrid sol–gel coatings for metal corrosion protection: a review of recent progress, J. Coat. Technol. Res. 12 (2015) 1–35.

[10] S.K. Rhee, Porosity-Thermal conductivity correlations for ceramic materials, Mater. Sci. Eng. 20 (1975) 89–93.

[11] A. Rosencwaig, A. Gersho, Theory of the photoacoustic effect with solids, J. Appl. Phys. 47 (1976) 65–69.

[12] C.A. Bennett, R.R. Patty, Thermal wave interferometry: a potential application of the photoacoustic effect, Appl. Opt. 21 (1) (1982) 49–58.

[13] M. Maliński, Ł. Chrobak, A. Patryn, Theoretical and Experimental Studies of a Plasma Wave Contribution, Acta Acust. Acust. 95 (2009) 60–64.

[14] Ł. Chrobak, M. Maliński, A. Patryn, Influence of Plasma Waves on the Photoacoustic Signal of Silicon Samples, Int. J. Thermophys. 32 (9) (2011) 1986–1997.

[15] Ł. Chrobak, M. Maliński, Determination of the Transport and Thermal Properties of Silicon Samples from the Phase-Lag and Sf/Sr Methods, Archives of Acoustics 34 (4) (2009) 727–734.

[16] M. Maliński, Temperature distribution formulae-applications in photoacoustics, Archives of Acoustics 27 (3) (2002) 217–228.

[17] I. Riech, M. Zambrano, A. Abelenda, F. Maldonado, A. Rojas-Marroquín, J. Jaime, A. Calderón, E. Marín, Evaluation of thin films intermixing by photoacoustic spectroscopy, Thin Solid Films 735 (2021), 138871.

[18] A. Kesmia, F.Z. Satour, A. Zegadi, Spectral absorption coefficient extraction of an unknown layer from photoacoustic measurements of multilayered semiconductors, Infrared Phys. Technol. 108 (2020), 103348.

[19] D.S. Volkov, O.B. Rogova, M.A. Proskurnin, Photoacoustic and photothermal methods in spectroscopy and characterization of soils and soil organic matter, Photoacoustics 17 (2020), 100151.

[20] P.-E. Nordal, S.O. Kanstad, Photothermal Radiometry, Phys. Scr. 20 (5–6) (1979) 659–662.

[21] A. Mandelis, Laser infrared photothermal radiometry of semiconductors: principles and applications to solid state electronics, Solid State Electron. 42 (1) (1998) 1–15.

[22] S. Pham Tu Quoc, G. Cheymol, A. Semerok, "New contactless method for thermal diffusivity measurements using modulated photothermal radiometry", Review of Scientific Instruments 85 (2014), 054903.

[23] Ł. Chrobak, M. Maliński, Investigations of the possibility of determination of thermal parameters of Si and SiGe samples based on the photo thermal radiometry technique, Infrared Phys. Technol. 89 (2018) 46–51.

[24] K. Dorywalski, Ł. Chrobak, M. Maliński, Comparative studies of the optical absorption coefficient spectra in the implanted layers in silicon with the use of nondestructive spectroscopic techniques, Metrology and Measurement Systems 27 (2) (2020) 323–337.

[25] Ł. Chrobak, M. Maliński, On Investigations of the Optical Absorption Coefficient of Gold and Germanium Implanted Silicon with the Use of the Non-destructive Contactless Photo Thermal Infrared Radiometry, J. Electron. Mater. 48 (8) (2019) 5273–5278.

[26] G. Leahu, E. Petronijevic, R. Li, A. Belardini, T. Cesca, G. Mattei, C. Sibilia, Diffracted Beams from Metasurfaces: High Chiral Detectivity by Photothermal Deflection Technique, Adv. Opt. Mater. 9 (21) (2021) 2100670.

[27] H. Cabrera, D. Korte, H. Budasheva, B.A.N. Asbaghi, S. Bellucci, Through-Plane and In-Plane Thermal Diffusivity Determination of Graphene Nanoplatelets by Photothermal Beam Deflection Spectrometry, Materials 14 (23) (2021) 7273.

[28] D. Korte, M. Franko, Application of complex geometrical optics to determination of thermal, transport, and optical parameters of thin films by the photothermal beam deflection technique, J. Opt. Soc. Am. A 32 (1) (2014) 61–74.

[29] D. Korte, F. Mladen, "Application of complex geometrical optics to determination of thermal, transport, and optical parameters of thin films by the photothermal beam deflection technique", Journal of the Optical Society of America, A, Optics, image science, and vision. 32 (1) (2015) 61–74.

[30] M. Abdelhamid, D. Korte, H. Cabrera, O. Pliekhova, Z. Ebrahimpour, U.L. Štangar, M. Franko, Thermo-optical characterization of cu- and ZR-modified TiO2 photocatalysts by beam deflection spectrometry, Applied Sciences (Switzerland) 11 (22) (2021) 10937.

[31] W. Jackson, N.M. Amer, Piezoelectric photoacoustic detection: theory and experiment, J. Appl. Phys. 51 (6) (1980) 3433–13353.

[32] M. Maliński, Determination of the thermal diffusivity from the piezoelectric photoacoustic spectra, Physica Status Solidi (a) 198 (1) (2003) 169–175.

[33] H. Zheng, Y. Li, Y. Chen, Z. Wang, J. Dai, Experimental Research on Measuring the Concentration of CO2 in Gas-Liquid Solution Based on PZT Piezoelectric-Photoacoustic Spectroscopy, Sensors 22 (3) (2022) 936.

[34] K. Dubyk, A. Pastushenko, T. Nychyporuk, R. Burbelo, M. Isaiev, V. Lysenko, Thermal conductivity of silicon nanomaterials measured using the photoacoustic technique in a piezoelectric configuration, J. Phys. Chem. Solid 126 (2019) 267–273.

[35] K. Dubyk, R. Burbelo, M. Isaiev, Features of photoacoustic response formation in systems with interface nanostructured solid / liquid, Journal of Nano- and Electronic Physics 10 (5) (2018) 05007.

[36] J. Zakrzewski, M. Maliński, A. Bachiri, K. Strzałkowski, Photothermal determination of the optical and thermal parameters of CdxZn1-xSe mixed crystals, Mater. Sci. Eng. B 271 (2021), 115305.

[37] K. Strzałkowski, "The composition effect on the thermal and optical properties across CdZnTe crystals"Journal of Physics D, Appl. Phys. 49 (2016), 435106.

[38] K. Strzałkowski, D. Dadarlat, Simultaneous thermal and optical characterization of semiconductor materials exhibiting high optical absorption by photopyroelectric spectroscopy, Measurement 184 (2021), 109956.

[39] K. Strzałkowski, Thermal properties of selected II–VI semiconductors determined by photopyroelectric calorimetry technique, J. Therm. Anal. Calorim. 145 (2021) 227–244.

[40] D. Singh, K. Strzałkowski, A. Abouais, A. Alaoui-Belghiti, Study of the Thermal Properties and Lattice Disorder Effects in CdTe–Based Crystals: CdBeTe, CdMnTe, and CdZnTe, Crystals 12 (2022) 1555.

[41] N.C. Fernelius, Extension of the Rosencwaig-Gersho photoacoustic spectroscopy theory to include effects of a sample coating, J. Appl. Phys. 51 (1) (1980) 650–654.

[42] M. Maliński, L. Bychto, J.L. Nzodoum Fotsing, K. Junge, A. Patryn, The model of a thin semiconductor layer on the thermally thick semiconductor backing, J. Phys. IV 109 (2004) 29–40.

[43] P. Rodič, J. Katić, D. Korte, P.M. Desimone, M. Franko, S.M. Ceré, M. Metikoš-Huković, I. Milošev, The Effect of Cerium Ions on the Structure, Porosity and Electrochemical Properties of Si/Zr-Based Hybrid Sol-Gel Coatings Deposited on Aluminum, Metals 8 (4) (2018) 248.

[44] M. Maliński, "Photoacoustics and photoacoustic spectroscopy of semiconductor materials", Technical University of Koszalin Publishing, 2004, ISSN 0239-7129.

[45] L. Klein, M. Aparicio, A. Jitianu, eds., "Handbook of Sol-Gel Science and Technology: Processing, Characterization and Applications", 2nd ed., Springer International Publishing, 2018.

[46] I. Milošev, D. Hamulić, P. Rodič, C.h. Carrière, S. Zanna, H. Budasheva, D. Korte, M. Franko, D. Mercier, A. Seyeux, P. Marcus, Siloxane polyacrylic sol-gel coatings with alkly and perfluoroalkyl chains: Synthesis, composition, thermal properties and log-term corrosion protection, Appl. Surf. Sci. 574 (2022), 151578.

[47] C.A. Hernández-Barrios, J.A. Saavedra, S.L. Higuera, A.E. Coy, F. Viejo, Effect of cerium on the physicochemical and anticorrosive features of TEOS-GPTMS sol-gel coatings deposited on the AZ31 magnesium alloy, Surf. Interfaces 21 (2020), 100671.

[48] M. Feuillade, C. Croutxé-Barghorn, C. Carré, Investigation of inorganic network formation in photopatternable hybrid sol–gel films by 29Si liquid NMR, J. Non Cryst. Solids 352 (4) (2006) 334–341.

[49] P. Rodič, I. Milošev, M. Lekka, F. Andreatta, L. Fedrizzi, Corrosion behaviour and chemical stability of transparent hybrid sol-gel coatings deposited on aluminium in acidic and alkaline solutions, Prog. Org. Coat. 124 (2018) 286–295.

[50] P. Rodič, J. Iskra, I. Milošev, Study of a sol–gel process in the preparation of hybrid coatings for corrosion protection using FTIR and 1H NMR methods, J. Non Cryst. Solids 396–397 (2014) 25–35.
[51] Ł. Chrobak, M. Maliński, Design and Optimization of the Photoacoustic Cell for Nondestructive Photoacoustic Spectroscopy, Nondestructive Testing and Evaluation 28 (1) (2013) 17–27.
[52] Ł. Chrobak, M. Maliński, Comparison of the CRLC Models Describing the Helmholtz Type Cells for the Nondestructive Photoacoustic Spectroscopy, Metrology and Measurement Systems 21 (3) (2014) 545–552.
[53] M.N. Popovic, M.V. Nesic, S. Ciric-Kostic, M. Zivanov, D.D. Markushev, M. D. Rabasovic, S.P. Galovic, Helmholtz Resonances in Photoacoustic Experiment with Laser-Sintered Polyamide Including Thermal Memory of Samples, Int. J. Thermophys. 37 (12) (2016) 116.
[54] K. Sathiyamoorthy, M.C. Kolios, Experimental design and numerical investigation of a photoacoustic sensor for a low-power, continuous-wave, laser-based frequency-domain photoacoustic microscopy, J. Biomed. Opt. 24 (12) (2019), 121912.
[55] B. Huan, H. Huan, L. Liu, Sensitivity dependence of optical parameters in a photoacoustic cell analyzed with a 2-D thermoelastic approximation, Opt. Commun. 497 (2021), 127171.
[56] J. H. Williams, "Quantifying measurement", Morgan & Claypool Publishers (2016), Online ISBN: 978-1-6817-4433-9, Print ISBN: 978-1-6817-4432-2.
[57] L. Kirkup, R. B. Frenkel, "An introduction to uncertainty in measurement: using the GUM (guide to the expression of uncertainty in measurement)", Cambridge: Cambridge University Press (2010), Online ISBN: 978-0-5117-5553-8.
[58] Ł. Chrobak, D. Korte, H. Budasheva, M. Maliński, P. Rodič, I. Milošev, S. Janta-Lipińska, Investigations of the thermal parameters of hybrid sol-gel coatings using nondestructive photothermal techniques, Energies 15 (11) (2022) 4122.